Supplement of Atmos. Chem. Phys., 25, 143–156, 2025
https://doi.org/10.5194/acp-25-143-2025-supplement

Atmospheric Chemistry and Physics Open Access

Supplement of

Long-term observations of black carbon and carbon monoxide in the Poker Flat Research Range, central Alaska, with a focus on forest wildfire emissions

Takeshi Kinase et al.

Correspondence to: Takeshi Kinase (tkinase@jamstec.go.jp)

Time series of CO mixing ratio observed at PFRR from ground based observation (our study) and aircraft observation by NOAA

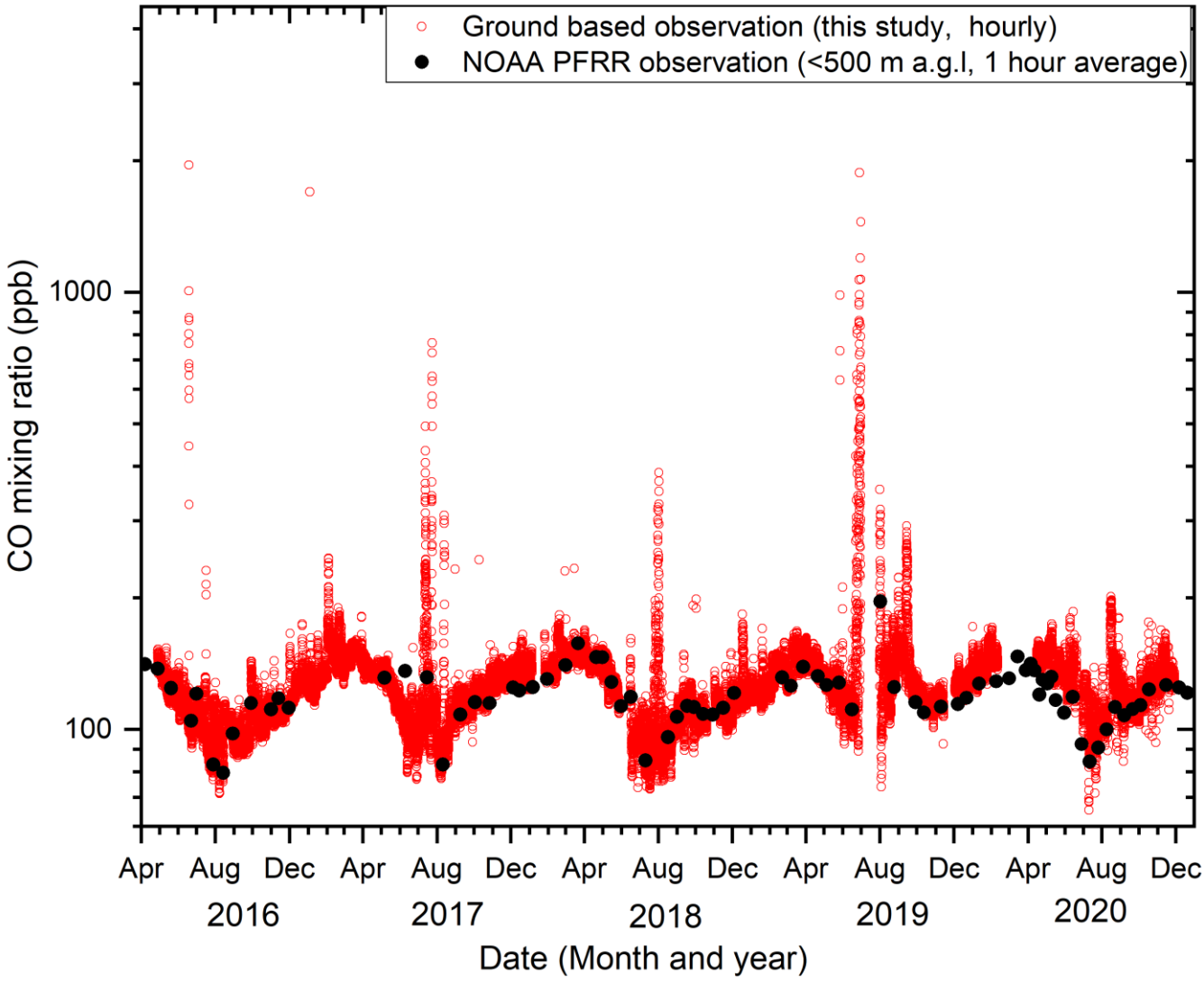

Figure S1. Time series of CO mixing ratios observed at PFRR. Red circles show the hourly ground-based observation (this study), and black points show the averages of individual aircraft observations (below 500 m a.g.l) made by NOAA Global Monitoring Laboratory approximately every 3 weeks. Because our observations were done continuously with a high-temporal resolution, several high-concentration peaks could be captured.

A map of FRP smaller than 0.3 Mw and panorama photo around the observation laboratory

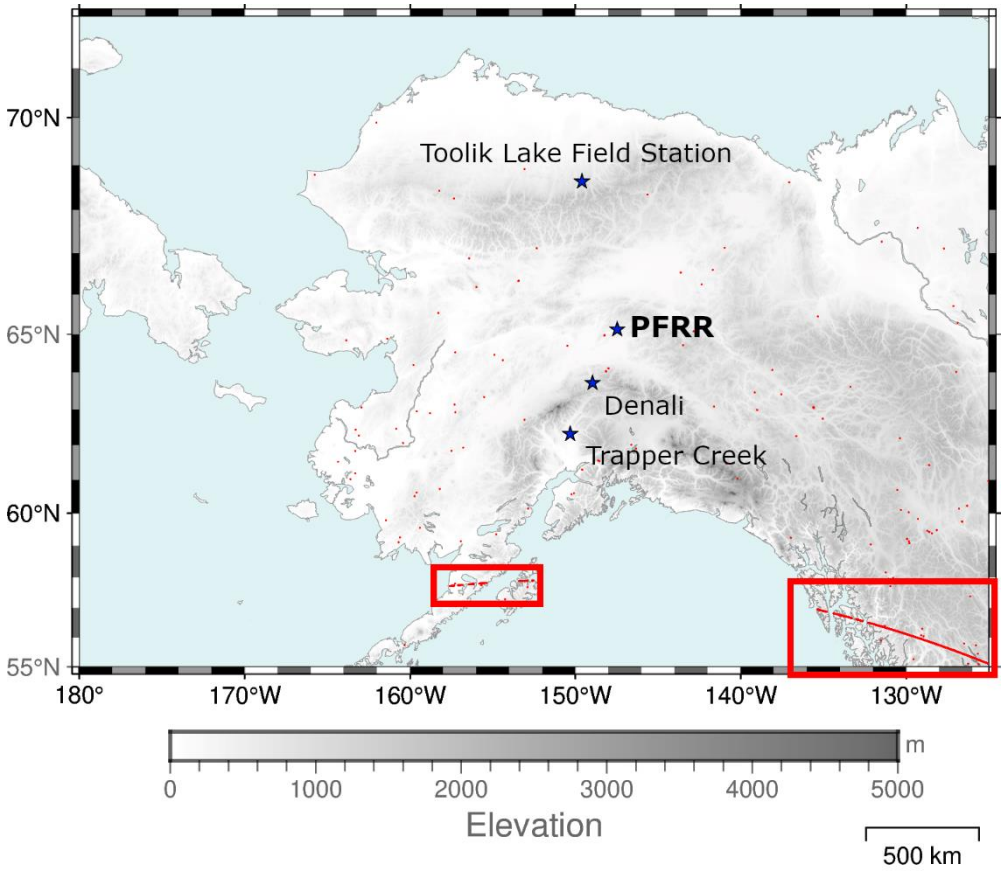

Figure S2. A map of hot spots smaller than 0.3 MW. We can find outliers indicated by two red rectangles. To avoid these artefacts, we selected FRP values larger than 0.3 MW in this study.

Time series of BC mass concentration observed at PFRR and other sites

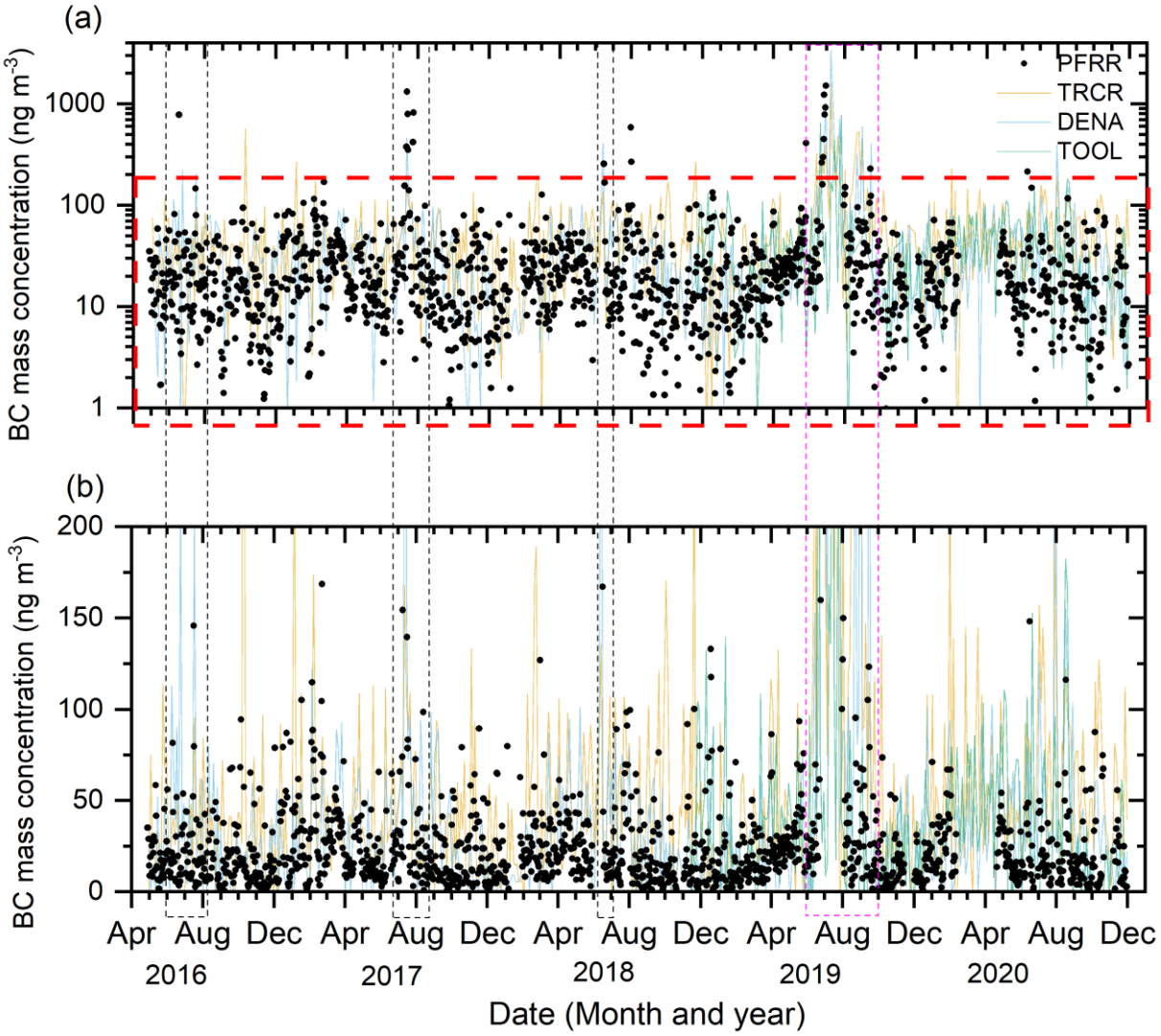

Figure S3. (a)Time series of daily averages and daily observation of BC mass concentrations observed at PFRR, TRCR, DENA, and TOOL. The black points show the observation results at PFRR, and individual coloured lines show the observation results for TRCR, DENA, and TOOL as indicated by legends to the right. Synchronised BC mass concentration peaks observed at PFRR and DENA are indicated by black dot boxes. Synchronised BC mass concentration peaks observed at PFRR, TRCR, DENA and TOOL are indicated by a pink dot box. To show the variation of BC mass concentrations in the low concentration level, an expanded plot for low BC mass concentrations ranging between 0 and 200 ng m^{-3} was shown in (b) by a linear scale.

The correlation plot observed by COSMOS at PFRR and the FLEXPART-WRF simulation

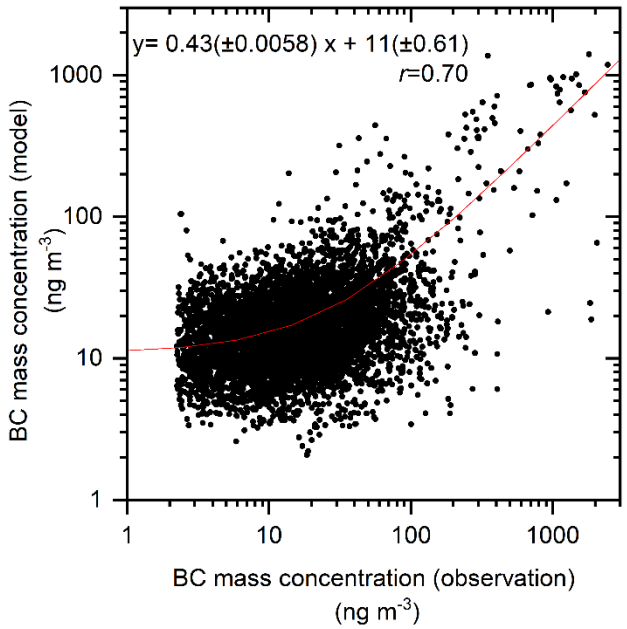

Figure S4. Correlation plot between 6-hour averages of observed hourly BC mass concentration and simulated 6-hourly BC mass concentration by FLEXPART-WRF. A result of least square regression in linear scale is shown in a red curve. Numbers in parentheses indicate standard errors of a slope and an intercept of this regression.

Examples of PES footprints and contributions of BC from biomass burning emissions at 12:00 on 27 June 2019.

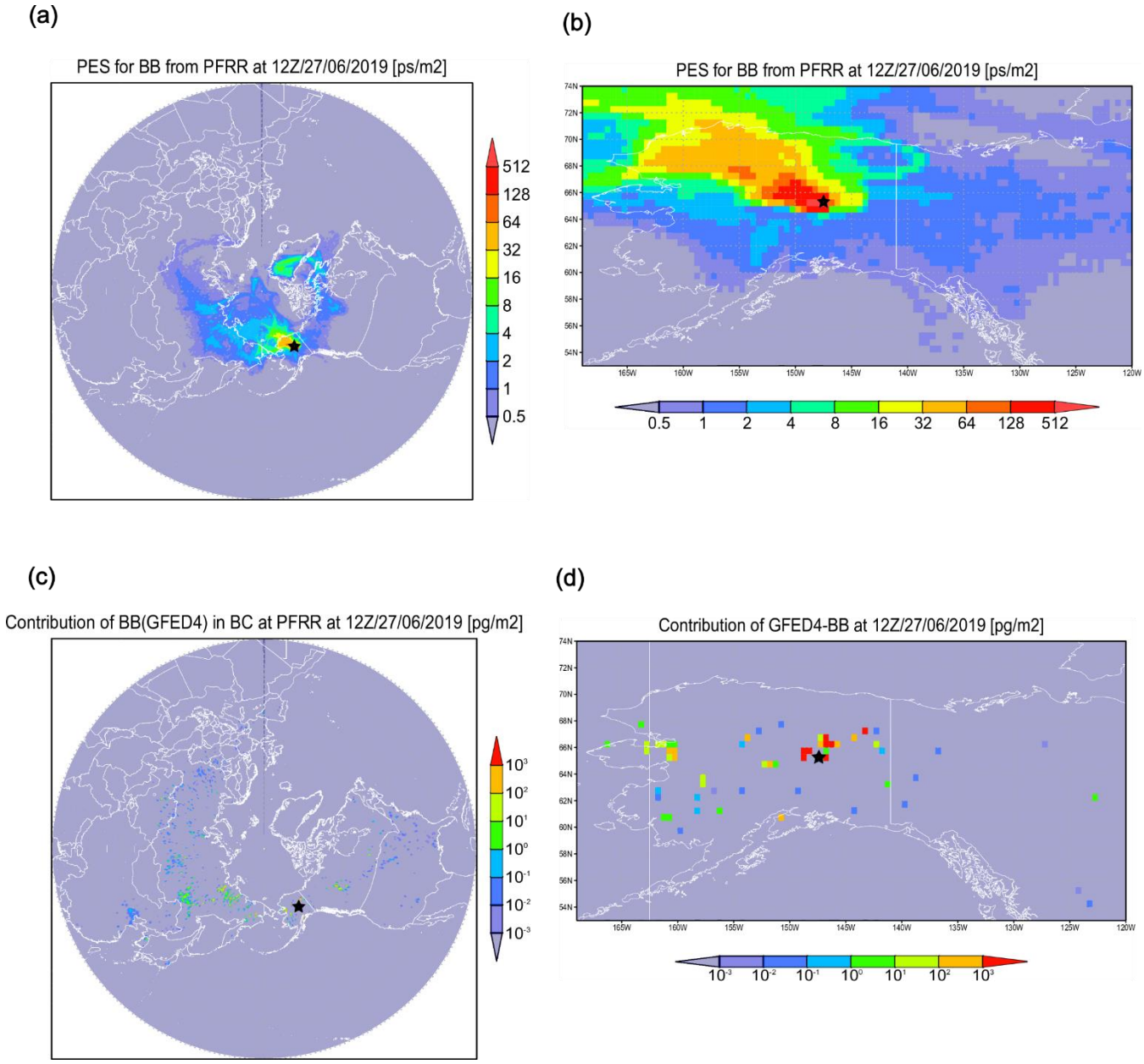

Figure S5. Examples of (a) a PES footprint calculated by the FLEXPART-WRF on a hemispheric scale, (b) that focused on Alaska and Western Canada, (c) a possible BC emission contribution from biomass burning estimated using PES and GFED inventory on a hemispheric scale, and (d) that focused on Alaska and Western Canada at 12:00 on 27 June 2019. In this case, high BC concentration (1611 ng m^{-3} on hourly average) was observed at PFRR and most BC came from forest wildfires around PFRR. Star marks indicate the PFRR location.

Examples of PES footprints and contributions of BC from biomass burning emissions at 00:00 on 12 July 2017.

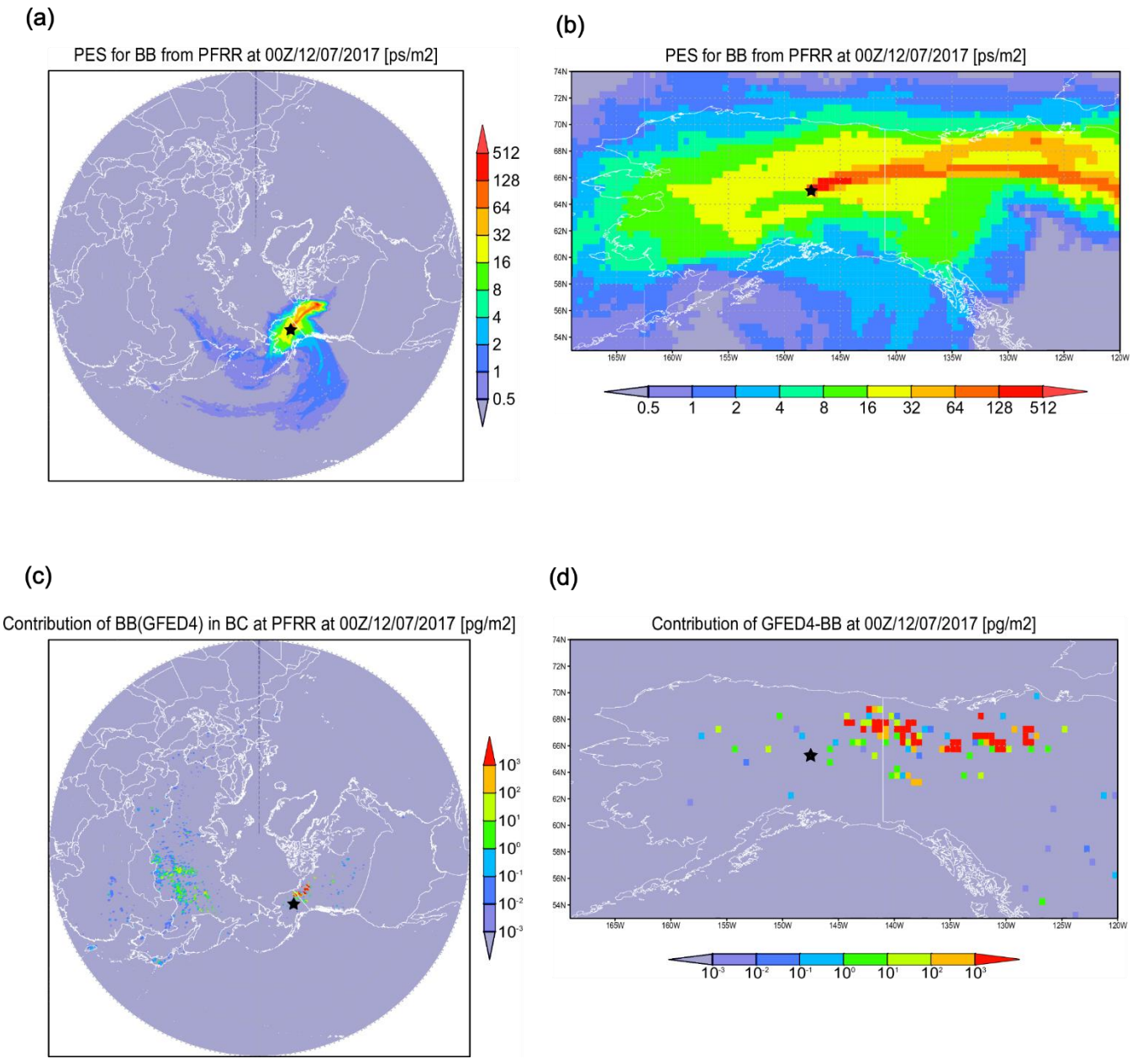

Figure S6. Same as Figure S5 but at 00:00 on 12 July 2017. In this case, high BC concentration (204 ng m^{-3} on hourly average) was observed at PFRR and most BC came from forest wildfires in western Canada and partly Alaska. Star marks indicate the PFRR location.

Table S1. Main configuration parameters adopted for the FLEXPART-WRF simulations in this study.

WRF-ARW 4.2.1 configuration	
Initial and boundary conditions	ECMWF ERA5 (Pressure-levels), hourly
PBL parameterization	MYNN level 2.5
Shortwave and longwave radiation	RRTMG
Land surface	Noah-MP
Microphysicis	Morrison 2-moment
Convection	Grell 3D ensemble
Maximum height	10 hPa
Domain size (x,y and z)	399x399x44 grids (mass points)
Map projection	Polar Stereographic centered at the North Pole

FLEXPART-WRF 3.3 configuration	
LSUBGRID	1 (enables subgrid terrain effect)
TURB_OPTION	1 (PBL turbulent mixing is calculated in the same manner with FLEXPART)
CBL_OPTION	1 (skewed option for the convective PBL)
SFC_OPTION	1 (PBL height is taken from WRF)
WIND_OPTION	1 (mass-weighted, time-averaged wind U,V and W calculated in WRF)
Interval of input data	hourly
Density of BC	1400 kg m^{-3}
Mean diameter of BC	0.25 μm
Standard deviation of BC size distribution	1.25
Release height	100-200 m A.G.L.
Number of particles	40,000
Output grids (horizontal)	180°W-180°E, 20°-90°N, every 0.5°
Output grids (vertical)	11 layers (50, 100, 150, 200, 500, 1000, 1500, 2000, 2500, 3000, 20000 m A.G.L.)

Table S2. Root Mean Square Error (RMSE) of the 6-hour averaged model calculated BC mass concentrations at PFRR. Model-calculated BC mass concentrations were estimated using the same footprint calculated by the FLEXPART-WRF model and different emission inventories.

Inventory	RMSE (ng m^{-3})
FINN v1.5 (Wiedinmyer et al., 2011))	35.8
FINN v2.5 (MODIS+VIIRS) (Wiedinmyer et al., 2023)	28.4
GFED v4.1s (Randerson et al., 2015)	**12.7**
GFAS v1.2 (Kaiser et al., 2012)	26.6
QFED v2.5r1 (https://portal.nccs.nasa.gov/datashare/iesa/aerosol/emissions/QFED/v2.5r1/)	21.9
FEER v1.0-G1.2 (Ichoku and Ellison, 2014)	31.0

Ichoku, C. and Ellison, L.: Global top-down smoke-aerosol emissions estimation using satellite fire radiative power measurements, Atmos. Chem. Phys., 14, 6643–6667, https://doi.org/10.5194/acp-14-6643-2014, 2014.

Kaiser, J. W., Heil, A., Andreae, M. O., Benedetti, A., Chubarova, N., Jones, L., Morcrette, J.-J., Razinger, M., Schultz, M. G., Suttie, M., and van der Werf, G. R.: Biomass burning emissions estimated with a global fire assimilation system based on observed fire radiative power, Biogeosciences, 9, 527–554, https://doi.org/10.5194/bg-9-527-2012, 2012.

Randerson, J. T., Van Der Werf, G. R., Giglio, L., Collatz, G. J., and Kasibhatla, P. S.: Global Fire Emissions Database, Version 4.1 (GFEDv4), https://doi.org/10.3334/ORNLDAAC/1293, 2015.

Wiedinmyer, C., Akagi, S. K., Yokelson, R. J., Emmons, L. K., Al-Saadi, J. A., Orlando, J. J., and Soja, A. J.: The Fire INventory from NCAR (FINN): a high resolution global model to estimate the emissions from open burning, Geoscientific Model Development, 4, 625–641, https://doi.org/10.5194/gmd-4-625-2011, 2011.

Wiedinmyer, C., Kimura, Y., McDonald-Buller, E. C., Emmons, L. K., Buchholz, R. R., Tang, W., Seto, K., Joseph, M. B., Barsanti, K. C., Carlton, A. G., and Yokelson, R.: The Fire Inventory from NCAR version 2.5: an updated global fire emissions model for climate and chemistry applications, Geoscientific Model Development, 16, 3873–3891, https://doi.org/10.5194/gmd-16-3873-2023, 2023.